Detection of External Rotor PMSM Inter-Turn Short Circuit Fault using Extended Kalman Filter

Ahmed Belkhadir, Remus Pusca, Raphael Romary, Driss Belkhayat, Youssef Zidani

Detection of External Rotor PMSM Inter-Turn Short Circuit Fault using Extended Kalman Filter

Ahmed Belkhadir *
Univ. Artois, UR 4025, Laboratoire Systèmes Electrotechniques et Environnement (LSEE), F-62400
Béthune, France.
Univ. Cadi Ayyad, P.O. Box 549, Laboratoire des Systèmes Electriques, Efficacité Energétique et Télécommunications (LSEEET),
Marrakesh, Morocco.
ahmed_belkhadir@ens.univ-artois.fr
ahmed.belkhadir@ced.uca.ma

Remus Pusca
Univ. Artois, UR 4025, Laboratoire Systèmes Electrotechniques et Environnement (LSEE), F-62400
Béthune, France.
remus.pusca@univ-artois.fr

Raphael Romary
Univ. Artois, UR 4025, Laboratoire Systèmes Electrotechniques et Environnement (LSEE), F-62400
Béthune, France.
raphael.romary@univ-artois.fr

Driss Belkhayat
Univ. Cadi Ayyad, P.O. Box 549, Laboratoire des Systèmes Electriques, Efficacité Energétique et Télécommunications (LSEEET),
Marrakesh, Morocco.
driss.belkhayat@uca.ma

Youssef Zidani
Univ. Cadi Ayyad, P.O. Box 549, Laboratoire des Systèmes Electriques, Efficacité Energétique et Télécommunications (LSEEET),
Marrakesh, Morocco.
y.zidani@uca.ma

***Abstract*— The presence of an inter-turn short circuit in electrical machines can lead to the complete shutdown of the system and cause disturbances in operation. In this paper, a diagnosis method for the detection of a stator inter-turn short circuit fault on an external rotor permanent magnet synchronous motor is proposed. The detection approach is based on the Extended Kalman Filter, which continuously estimates the different quantities of the machine. The designed technique is based on a comparison of the estimated and measured stator currents. An analysis of the signals resulting from the comparison is used to detect and locate the fault. Simulation results are presented to validate the proposed fault detection and diagnosis approach.**

Keywords*— *Inter-turn short circuit, fault detection and diagnosis, external rotor permanent magnet synchronous motor, extended Kalman filter.

I. INTRODUCTION

Nowadays, External Rotor Permanent Magnet Synchronous Motors (ER-PMSMs) comprise a very significant component of the drive systems used in the powertrains of hybrid and electric vehicle (HEV). Therefore, diagnosis and early detection of faults become crucial issues to ensure continuity of service. These techniques enable monitoring, fault detection, and isolation, as well as reconfiguration of the control strategy to protect the healthy parts of the machine [1].

ER-PMSMs are exposed to various types of magnetic (Permanent Magnet (PM)), mechanical (eccentricity, bearings, unbalance), and electrical (stator winding) faults that disturb the normal operation of the machine [2]. According to [3], stator winding faults are the predominant faults that appear in AC electrical machines, accounting for 36% to 66%, respectively, according the size of the motor. These types of faults appear as an imperceptible Inter-Turn Short Circuit (ITSC) fault, which expands very fast throughout the winding, potentially causing a ground fault of a Lack of Turns (LTs) faults [4].

Currently, several research has been conducted on Fault Detection and Diagnosis (FDD) methods in ER-PMSMs. The three most recognized approaches developed over the years are signal analysis methods, diagnosis employing mathematical modeling, and methods using techniques of artificial intelligence [5].

Inter-Turn Short Circuit (ITSC) can be detected by various techniques based on signals, models, and data. Among them, the FDD method performs a time domain analysis using adaptive observers to conduct a residual analysis between the estimated signals of the healthy and faulty model with the measured ones in healthy and faulty machine. This technique has the advantage of non-invasive methods without the need for additional sensors. The residual signal is usually compared to a threshold to avoid false alarms due to disturbances or uncertainty. In [6], an adaptive observer has been proposed to establish a system that can identify the ITSC fault condition in an induction machine. In [7], a detection algorithm based on the principal component approach and combined with a classical vector method yields results under real conditions.

The main objective of this paper is the implementation of a non-invasive time-domain ITSC fault detection technique for a closed-loop controlled ER-PMSM without sensor feedback using the Extended Kalman Filter (EKF). The residual signals generated by the FDD approach are employed by comparing the measured stator currents with those estimated using an EKF. Simulation and analysis are conducted to evaluate the proposed methodology in the ER-PMSM control system.

The organization of the paper is presented as follows. Section II presents the healthy and faulty ER-PMSM model. In section III, the extended Kalman filter synthesis is described. Then, the ITSC fault detection and diagnosis approach in closed-loop is developed. Finally, the robustness

of the FDD method is shown followed by tests and simulation results.

II. ER-PMSM Model

The detection of ITSC faults is particularly crucial since they might lead to more significant problems on the machine. To evaluate the FDD technique for the ER-PMSM with an ITSC fault, an accurate model including the faulty machine structure is required. Fig. 1 depicts the model of the ER-PMSM with an ITSC fault. The ER-PMSM is a double-layer fractional-slot concentrated-wound (FSCW) structure with 24 slots and 22 poles (24/22). Assuming the ITSC fault occurs in phase *a*, the circuit model is shown in Fig. 2.

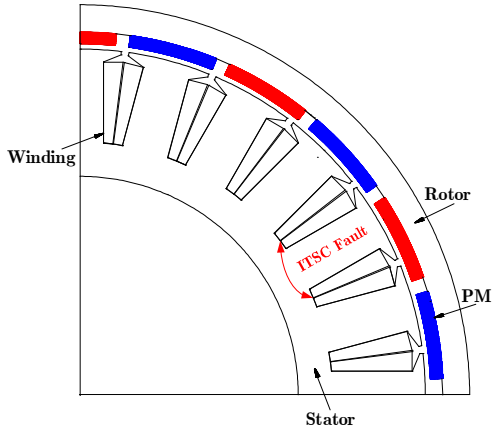

Fig. 1. ITSC ER-PMSM model.

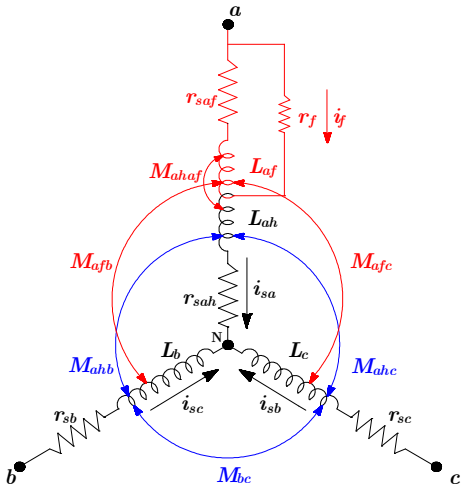

Fig. 2. Three phase electric model for ER-PMSM with ITSC fault.

A. Healthy ER-PMSM Model

The mathematical model of ER-PMSM can be represented as follows:

$$\left[V_{s,abc}\right]=\left[r_{s,abc}\right]\left[i_{s,abc}\right]+\left[L_{abc}\right]\frac{d}{dt}\left[i_{s,abc}\right]+\frac{d}{dt}\left[\phi_{r,abc}\right] \quad (1)$$

$$i_{sa}+i_{sb}+i_{sc}=0 \quad (2)$$

The product of the currents and the flux space phasor generate the electromagnetic torque:

$$\Gamma_e=\frac{3}{2}p\left(\bar{\phi}_s\wedge\bar{i}_s\right) \quad (3)$$

The flux and current can be determined with:

$$\bar{\phi}_s=\frac{2}{3}\left(\phi_{sa}+\phi_{sb}e^{j2\pi/3}+\phi_{sc}e^{j4\pi/3}\right) \quad (4)$$

$$\bar{i}_s=\frac{2}{3}\left(i_{sa}+i_{sb}e^{j2\pi/3}+i_{sc}e^{j4\pi/3}\right) \quad (5)$$

B. Faulty ER-PMSM Model

The ITSC fault is not necessarily straightforward, and equivalent resistance is used to model what remains of the insulation resistance between the shorted turns. The value of the resistance indicates the severity of the insulation fault. According to Fig. 2, the winding in which the fault occurs is thus divided into two parts. In reality, the evolution of the fault resistance r_f between infinity and zero is very fast when the machine is in the presence of an ITSC fault. It is therefore interesting to determine the behavior of the machine when this resistance is high enough not to induce an LTs fault [8] or the global destruction of the winding but also small enough for its impact to be perceptible on the currents absorbed by the ER-PMSM. The electrical equations written in two parts of phase A for a faulty three-phase ER-PMSM in the *abc* frame are provided by the following expressions [9]:

$$\begin{aligned}V_{aN}&=\left(r_{saf}+r_{sah}\right)i_{sa}+\left(L_{af}+L_{ah}+2M_{ahaf}\right)\frac{d}{dt}i_{sa}+\\&\left(M_{afb}+M_{ahb}\right)\frac{d}{dt}i_{sb}+\left(M_{afc}+M_{ahc}\right)\frac{d}{dt}i_{sc}-r_{saf}i_f-\\&\left(L_{af}+M_{ahaf}\right)\frac{d}{dt}i_f+\frac{d}{dt}\left(\phi_{rf}+\phi_{rah}\right)\end{aligned} \quad (6)$$

$$\begin{aligned}V_{bN}&=r_{sb}i_{sb}+L_b\frac{d}{dt}i_{sb}+\left(M_{afb}+M_{ahb}\right)\frac{d}{dt}i_{sa}+\\&M_{bc}\frac{d}{dt}i_{sc}-M_{afb}\frac{d}{dt}i_f+\frac{d}{dt}\phi_{rf}\end{aligned} \quad (7)$$

$$\begin{aligned}V_{cN}&=r_{sc}i_{sc}+L_c\frac{d}{dt}i_{sc}+\left(M_{afc}+M_{ahc}\right)\frac{d}{dt}i_{sa}+\\&M_{cb}\frac{d}{dt}i_{sb}-M_{afc}\frac{d}{dt}i_f+\frac{d}{dt}\phi_{rc}\end{aligned} \quad (8)$$

The following additional equation describes the mesh created by the ITSC fault:

$$\begin{aligned}0&=r_{saf}i_{sa}+\left(L_{af}+M_{ahaf}\right)\frac{d}{dt}i_{sa}+M_{afb}\frac{d}{dt}i_{sb}+\\&M_{afc}\frac{d}{dt}i_{sc}-\left(r_{saf}+r_f\right)i_f-L_{af}\frac{d}{dt}i_f+\frac{d}{dt}\phi_{rf}\end{aligned} \quad (9)$$

Where: ϕ_{rah}, ϕ_{rf}, ϕ_{rb} and ϕ_{rc} are respectively the flux linkages through the windings a_h, a_f, b and c, and which can be expressed by the following expressions:

$$\begin{cases}\phi_{rf}=Y_{coil}\phi_{PM}\cos\left(\theta\right)\\\phi_{rah}=\left(1-Y_{coil}\right)\phi_{PM}\cos\left(\theta\right)\\\phi_{rb}=\phi_{PM}\cos\left(\theta-2\pi/3\right)\\\phi_{rc}=\phi_{PM}\cos\left(\theta+2\pi/3\right)\end{cases} \quad (10)$$

The representation of the electromagnetic torque during the faulty state of the ER-PMSM can be represented as follows:

$$\boldsymbol{\Gamma}_e = \frac{3}{2} p \left(\bar{i}_s + \bar{i}_f' \right) \wedge \bar{\phi}_s \tag{11}$$

$$\bar{i}_f' = -\frac{1}{3} \boldsymbol{Y}_{coil} i_f \left(e^{j(\omega t + \varphi_f)} + e^{-j(\omega t + \varphi_f)} \right) \tag{12}$$

Taking into account the polarity of the ER-PMSM, the actual configuration of the winding, and the ITSC fault, the different elements are presented in the Appendix. We will use the following expressions where the coefficient μ describes the relative number of short-circuited turns:

$$\mu = \frac{N_f}{N_T} \tag{13}$$

Considering that the fault occurs in an elementary coil, the fraction of N_f in this coil over the N_T is:

$$\boldsymbol{Y}_{coil} = p \frac{N_f}{N_T} = p\mu \tag{14}$$

C. Analytical Identification of ER-PMSM Parameters

The identification and determination of the FSCW ER-PMSM parameters are based on the methodologies developed in [8] and [10].

$$\boldsymbol{L}_{ji} = \left(N_T \right)^2 R_s L_{axe} K_w \int_0^{2\pi} F_{distribution,j} \left(\theta_s \right) \wp \left(\theta_s \right) F_{w,i} \left(\theta_s \right) d\theta_s \tag{15}$$

$$\boldsymbol{L}_{ji} = \frac{\phi_a \left(t \right)}{i_{sa} \left(t \right)} \quad ; \boldsymbol{M}_{ji} = \frac{\phi_{ab} \left(t \right)}{i_{sa} \left(t \right)} \tag{16}$$

The healthy and faulty resistances and inductances are calculated from the following expressions:

$$\begin{cases} r_{saf} = \mu r_{sa} \\ r_{sah} = \left(1 - \mu \right) r_{sa} \end{cases} \tag{17}$$

$$\boldsymbol{L}_{af} = \boldsymbol{Y}_{coil}{}^2 \boldsymbol{L}_{coil} \tag{18}$$

$$\begin{aligned} \boldsymbol{L}_{ah} = {} & \left(p - 1 \right) \left[\boldsymbol{L}_{coil} + \left(p - 2 \right) \boldsymbol{M}_{coil} \right] + \\ & \left(1 - \boldsymbol{Y}_{coil} \right)^2 \boldsymbol{L}_{coil} + 2 \left(1 - \boldsymbol{Y}_{coil} \right) \left(p - 1 \right) \boldsymbol{M}_{coil} \end{aligned} \tag{19}$$

$$\begin{aligned} \boldsymbol{M}_{ahaf} = {} & \boldsymbol{Y}_{coil} \left(1 - \boldsymbol{Y}_{coil} \right) \boldsymbol{L}_{coil} + \\ & \boldsymbol{Y}_{coil} \left(p - 1 \right) \boldsymbol{M}_{coil} \end{aligned} \tag{20}$$

$$\boldsymbol{M}_{afb} = \boldsymbol{M}_{afc} = \boldsymbol{Y}_{coil} \left(\boldsymbol{M}_{ab} / p \right) \tag{21}$$

$$\boldsymbol{M}_{ahb} = \boldsymbol{M}_{ahc} = \left[\left(p - 1 \right) + \left(1 - \boldsymbol{Y}_{coil} \right) \right] \left(\boldsymbol{M}_{ab} / p \right) \tag{22}$$

III. Extended Kalman Filter

The EKF is an approach for estimating the state of a system characterized by a stochastic model, which is based on a discrete model of a process, taking into consideration the noise and errors of the modeling. The EKF must be able to describe the system state of the ER-PMSM. Fig. 3 depicts the schematic diagram of the EKF observing the state of the system.

Given the following linear, stochastic and stationary model:

$$\begin{cases} \boldsymbol{x}_{[K+1]} = \boldsymbol{A}_d \boldsymbol{x}_{[K]} + \boldsymbol{B}_d \boldsymbol{u}_{[K]} + \boldsymbol{w}_{[K]} \\ \boldsymbol{y}_{[K]} = \boldsymbol{C}_d \boldsymbol{x}_{[K]} + \boldsymbol{\lambda}_{[K]} \end{cases} \tag{23}$$

Where: A_d, B_d and C_d are the control and observation transition matrices, respectively. w and λ are the state and measurement noise sequences, respectively, which are presumed to be white, Gaussian, decorrelated, zero-mean noises with known covariances. Before implementing the EKF, it is essential to discretize the model by conducting a limited expansion for a small sampling period T_e [11]. The nonlinear representation is given by the following expression:

$$\begin{cases} \boldsymbol{x}_{[K+1]} = \boldsymbol{f} \left(\boldsymbol{x}_{[K]}, \boldsymbol{u}_{[K]} \right) + \boldsymbol{w}_{[K]} \\ \boldsymbol{y}_{[K]} = \boldsymbol{h} \left(\boldsymbol{x}_{[K]} \right) + \boldsymbol{\lambda}_{[K]} \end{cases} \tag{24}$$

The execution of the EKF begins with the phase of predicting the state $x_{[K+1]}$ based on the knowledge of the previous state. The model (24) allows the following expressions:

$$\hat{\boldsymbol{x}}_{[K+1|K]} = \boldsymbol{f} \left(\hat{\boldsymbol{x}}_{[K|K]}, \boldsymbol{u}_{[K]} \right) \tag{25}$$

The covariance matrix of the estimation error must be essentially predicted to determine the correction phase of the estimator. The covariance matrix of the prediction error is given by the following expression:

$$\boldsymbol{P}_{[K+1|K]} = \boldsymbol{F}_{[K]} \boldsymbol{P}_{[K|K]} \boldsymbol{F}_{[K]}^T + \boldsymbol{Q} \tag{26}$$

Where F is the Jacobian matrix of the system, which allows for linearizing the mathematical model of the ER-PMSM, and Q is the covariance matrix.

$$\boldsymbol{F}_{[K]} = \left. \frac{\partial \boldsymbol{f} \left(\boldsymbol{x}_{[K]}, \boldsymbol{u}_{[K]} \right)}{\partial \boldsymbol{x}} \right|_{\boldsymbol{x} = \hat{\boldsymbol{x}}_{[K+1|K]}} \tag{27}$$

$$\boldsymbol{Q} = \begin{bmatrix} 1e-3 & 0 & 0 & 0 & 0 \\ 0 & 1e-3 & 0 & 0 & 0 \\ 0 & 0 & 1e-2 & 0 & 0 \\ 0 & 0 & 0 & 1e-5 & 0 \\ 0 & 0 & 0 & 0 & 1e-5 \end{bmatrix} \tag{28}$$

The prediction of the covariance matrix of the estimation error allows us to determine the Kalman gain characterizing the correction phase of the estimator. The calculation of the matrix K will be done for each sampling step according to the following expression:

$$\mathbf{K}_{[K+1]} = \boldsymbol{P}_{[K+1|K]} \boldsymbol{H}^T \left(\boldsymbol{H} \boldsymbol{P}_{[K+1|K]} \boldsymbol{H}^T + \boldsymbol{R} \right)^{-1} \tag{29}$$

Where R is the covariance matrix.

$$\boldsymbol{R} = \begin{bmatrix} 15e-1 & 0 \\ 0 & 15e-1 \end{bmatrix} \tag{30}$$

$$\boldsymbol{H} = \left. \frac{\partial \boldsymbol{h} \left(\boldsymbol{x}_{[K]} \right)}{\partial \boldsymbol{x}} \right|_{\boldsymbol{x} = \hat{\boldsymbol{x}}_{[K+1|K]}} = \begin{bmatrix} 1 & 0 & 0 & 0 & 0 \\ 0 & 1 & 0 & 0 & 0 \end{bmatrix} \tag{31}$$

The identification of the correction matrix ensures the updates of the predicted state as follows:

$$\hat{x}_{[K+1|K+1]} = \hat{x}_{[K+1|K]} + \mathbf{K}_{[K+1]}\left(y_{[K+1]} - H\hat{x}_{[K+1|K]}\right) \quad (32)$$

$y_{[K+1]}$ represents the vector of measured conditions. The error covariance matrix must also be updated at each sampling step to ensure that the corrective phase and estimated state variables are updated.

$$P_{[K+1|K+1]} = \left(I - \mathbf{K}_{[K+1]}H\right)P_{[K+1|K]} \quad (33)$$

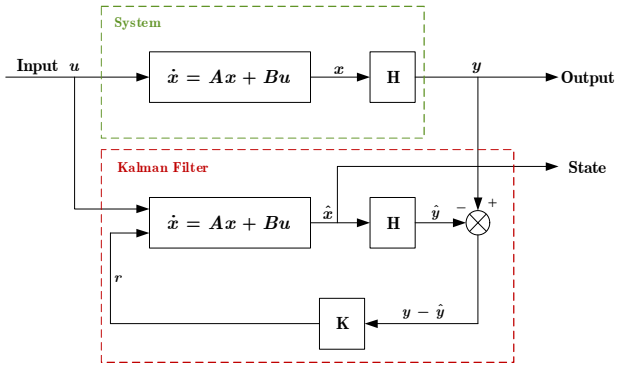

Fig. 3. Structure of the Kalman filter estimator.

IV. ITSC Fault Detection and Diagnosis Approach

The diagnosis of the ER-PMSM represents a significant lever to increase the availability of the machine and to ensure the continuity of service in the presence of the ITSC fault. The most important task in diagnosis activity is the detection and localization of the fault. In order to detect ITSC faults that can occur in the machine, the three-phase stator currents can be used as a tool for detection. Observation-based FDD approaches focus on the design of residuals that will be used as indicators of ITSC fault. The principle of this method resides in the exploitation of the state variables estimated by the EKF to generate a residual with a non-zero mean value in the faulty case. By exploiting the residuals, we derive signatures that will be used in the development of an algorithm enabling the detection and localization of the fault.

A. Residual Generation

EKF-based residual signal generation involves reconstructing the outputs of the ER-PMSM to compare the measured output vector to the estimated ones. Indeed, for the detection of the ITSC impacting the stator winding of phase *a*, three signals must be conducted. These signals are employed as flags to indicate the presence of the ITSC fault. It is then necessary to introduce detection thresholds to avoid false alarms.

$$r_a = \left|i_{sa} - \hat{i}_{sa}\right| \quad r_b = \left|i_{sb} - \hat{i}_{sb}\right| \quad r_c = \left|i_{sc} - \hat{i}_{sc}\right| \quad (34)$$

B. Threshlod Setting

The threshold is defined as the maximum value that the residual can reach in the absence of the ITSC fault and the presence of parametric load variations. The FDD method must not be susceptible to disturbances due to a variation in the stator resistance. The defined threshold can be described as the utmost value of r_a, r_b and r_c.

$$\varepsilon = Max\left[r_a, r_b, r_c\right] \quad (35)$$

C. Fault Detection

The detection is accomplished via the application of decision logic implementation able to generate signatures according to the comparison of the residual signals to the detection threshold ε [12].

$$Flag_n = \begin{cases} 0 & if \quad r_n < \varepsilon \\ 1 & if \quad r_n \geq \varepsilon \end{cases} \quad n = a, b, c \quad (36)$$

The circuit shown in Fig. 4 is charged to ensure the detection of the ITSC faults by examining the residual between the estimated and measured quantities. A Low Pass Filter (LPF) is used to extract the signal which will be compared to ε.

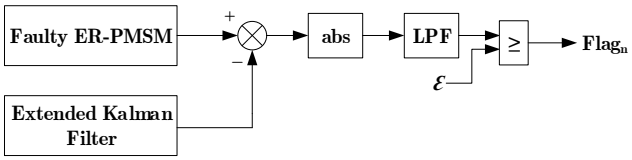

Fig. 4. EKF-based fault detection circuit.

V. Simulation Results

In this section, we present simulation results showing the operation of the ER-PMSM affected by an ITSC fault in its stator winding. The simulation test was performed using MATLAB/Simulink software. A 1.5 kW FSCW ER-PMSM is used with the parameters specified in Appendix (Table I). Fig. 5 illustrates the block diagram of the EKF-based control and the FDD structure under healthy and faulty states.

A. Test and Robustness of the EKF

To highlight the performance, robustness, and efficiency of the sensorless control algorithm, various tests are performed, i.e., no load start, load application, and reversal of the ER-PMSM speed rotation.

The following figures show the mechanical and electrical quantities of the sensorless control law in a healthy state. According to Fig. 6, it can be seen that the speed follows the reference after a transient and decreases slightly when a load is applied. The estimation reveals excellent performances and the effective monitoring of the estimated speed compared to the measured one and the reference. The electromagnetic torque is presented in Fig. 7, and demonstrates a fast dynamic with the application of the load at t = 2s. Fig. 8 depicts the stator currents measured and estimated by the EKF. Here the estimated currents converge to the measured ones. These results prove that the EKF has good performance in terms of convergence speed and accuracy. Also, the observer allows a reduction of the oscillations at the level of the electromagnetic torque.

B. Test and Robustness of the Detection Threshold

Parametric variations are a very critical requirement for an efficient FDD method. Indeed, to evaluate the robustness of the steady state detection, various load torque and stator resistance variations of the machine are applied. Fig. 9 illustrates that the residuals have small variations because of the robustness of the EKF. Based on these tests, the threshold value is determined after an analysis of the residual signal magnitudes. The threshold of ITSC fault detection and diagnosis is $\varepsilon = 0.2$ A.

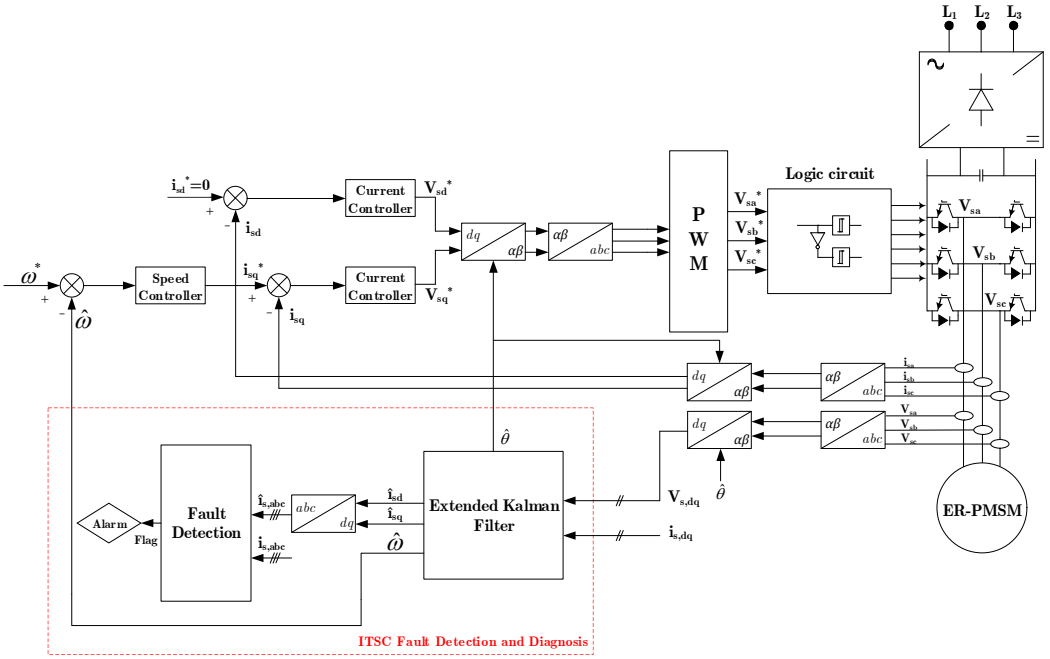

Fig. 5. Chart of the proposed strategy.

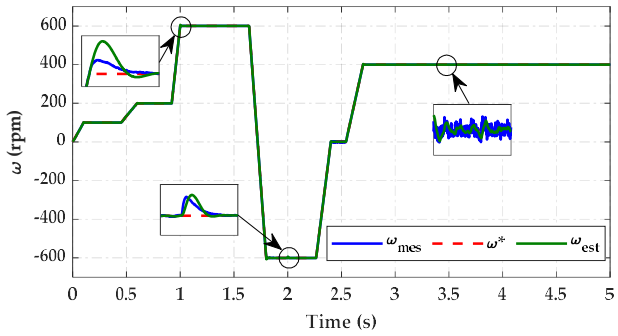

Fig. 6. Measured and estimated rotor speed (Benchmark test).

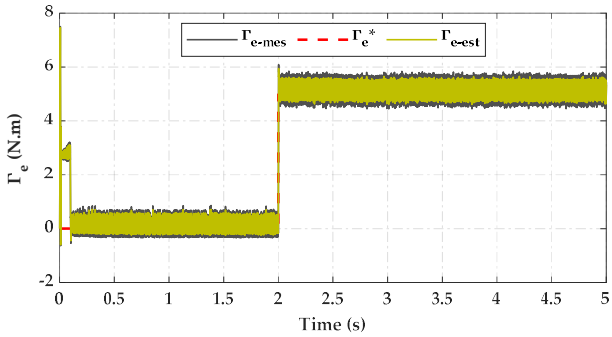

Fig. 7. measured and estimated electromagnetic torque.

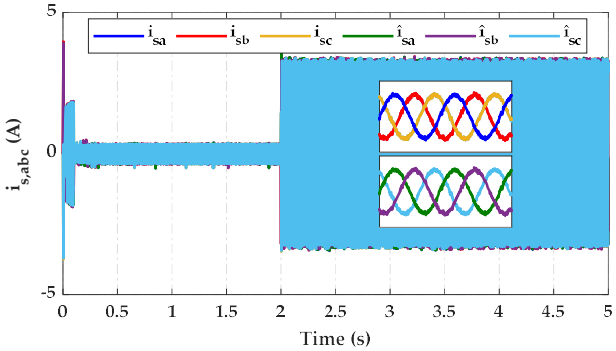

Fig. 8. Measured and estimated stator phase currents.

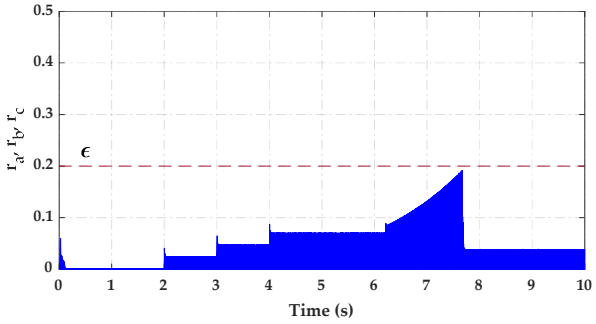

Fig. 9. Residual signals variations of a healthy ER-PMSM.

C. *Evaluation on the FDD Approach*

The ITSC fault was initialized by controlling the resistance r_f of the model proposed in Section II. The objective of this section is to study the behavior of the ER-PMSM with an ITSC fault as well as the robustness of the developed FDD approach. The control and detection structure is illustrated in Fig. 5. The various tests are performed under the scenario of an ITSC fault of 12.5% of the phase *a* winding, corresponding to an ITSC over one full coil $A_{full\text{-}coil}$, which results after 3.5s with a resistance r_f = 5Ω. The following analyses present the state variables of the ER-PMSM controlled by a current field-oriented control. Fig. 10 illustrates the evolution of the rotor speed in the presence of the fault. After the occurrence of the ITSC, ripples appear on the speed, which might lead to vibrations. According to the electromagnetic torque (Fig. 11), torque ripples are introduced after the occurrence of the fault, which causes the appearance of new harmonics. Fig. 12 shows the fault current, which is due to the presence of the ITSC. We notice that the value of the i_f current is important and can reach values that are inaccessible for the machine, which can induce the deterioration of the ER-PMSM. The stator currents are depicted in Fig. 13. A rather important asymmetry appeared during the fault condition. This asymmetry will be used to design the FDD approach bases

on EKF. The current i_{sq} (Fig. 14) also exhibits important oscillations once the fault appears. After presenting the impact of the ITSC fault on the various state variables of the ER-PMSM, we proceed to the implementation of the FDD method of the ITSC fault developed previously. The tests consist of generating the residuals to determine the specific signatures in the case of the ITSC fault. Fig. 15 and Fig. 16 depict the evolution of the residual r_a and its $flag_a$ signature in the case of the fault impacting the stator winding of phase a. The residual r_a remains very near zero in the absence of the ITSC (t<3.5s). From t = 3.5s, the magnitude of r_a change substantially and exceed the predefined threshold, which triggers an alarm indicating the presence of the ITSC fault.

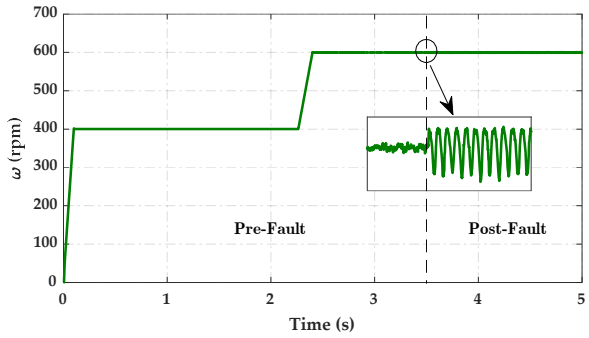

Fig. 10. Rotor speed under ITSC fault.

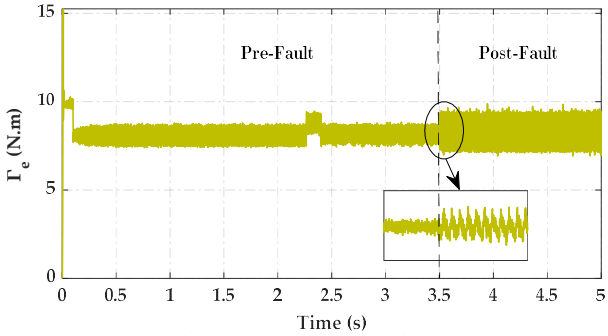

Fig. 11. Electromagnetic torque under ITSC fault.

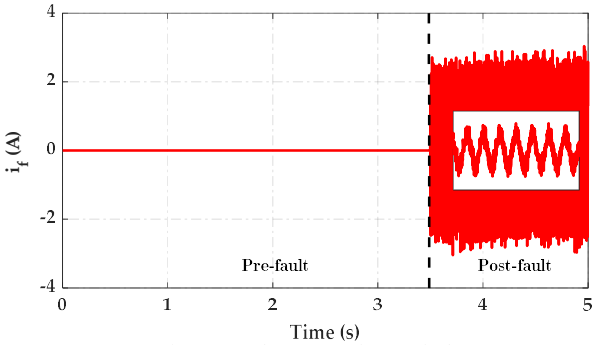

Fig. 12. Fault current of ITSC fault.

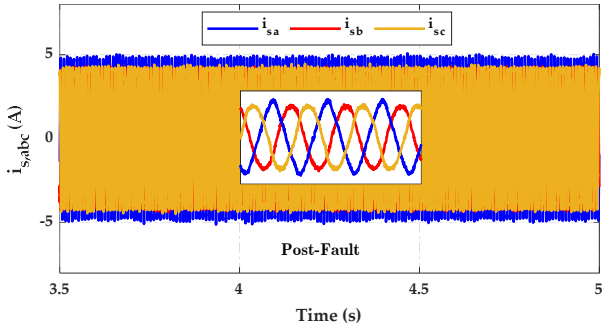

Fig. 13. Stator phase currents under ITSC fault.

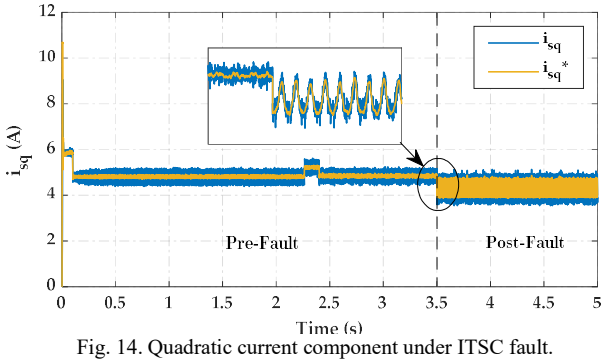

Fig. 14. Quadratic current component under ITSC fault.

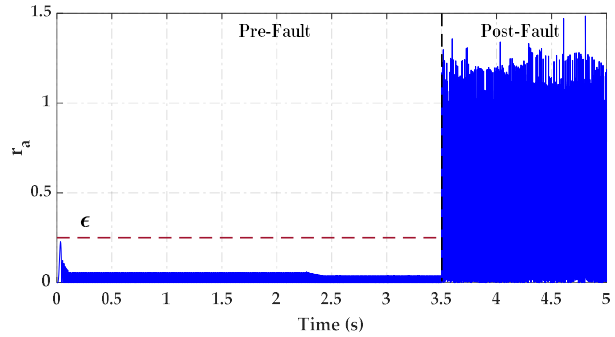

Fig. 15. Residual signal variation of phase A under ITSC fault.

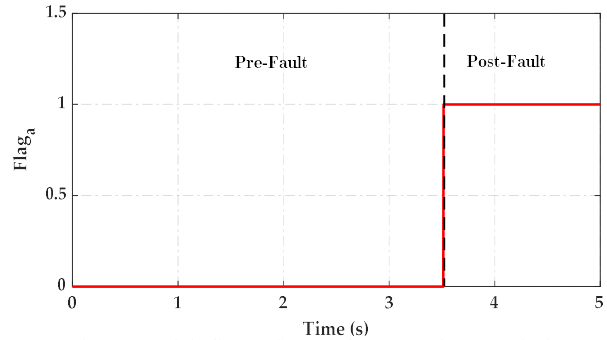

Fig. 16. Fault indicator $flag_a$ of phase A under ITSC fault.

VI. Conclusion

This paper presents the efficiency of the detection and diagnosis method based on the Extended Kalman Filter of an external rotor permanent magnet synchronous motor with an inter-turn short circuit fault. Taking the fault into account, a dynamic model of the ER-PMSM has been presented for the control of the machine in a closed loop control. The proposed detection strategy is based on the generation of residual signals by the EKF observer approach, which exhibits good estimation performance. From the detection point of view, the FDD technique is non-invasive and has a high sensitivity to faults. This allows the localization of the fault using observed signatures considering the tests under different loads and parametric variations. The effectiveness and robustness of the approach have been verified and validated by simulation. The proposed approach allows to improve preventive maintenance of the ER-PMSM and thus avoids unexpected failures and breakdowns.

The next step in the development of the work is to make the fault-tolerant control and detection approach more reliable throughout the fully electric drive train, including sensor faults.

APPENDIX

TABLE I. ER-PMSM PARAMETERS

Parameter	Value	Parameter	Value
Rated power P (kW)	1.5	Number of turns per coil N_T	22
Rated speed ω (rpm)	600	Stator resistances r_{sa}, r_{sb}, r_{sc} (Ω)	0.265
Frequency f (Hz)	110	Self inductances L_a, L_b, L_c (mH)	2.1041
DC bus voltage V_{DC} (V)	150	Mutual inductances M_{ab}, M_{bc}, M_{ac} (mH)	-0.0832
Rated current i_N (A_{RMS})	11	Self inductance of elementary coil L_{coil} (mH)	0.32
Rated torque Γ_e (N.m)	24	Mutual inductance between elementary coils M_{coil} (mH)	-0.0129
Number of poles $2p$	22	Magnet flux ϕ_{PM} (Wb)	0.1021

ϕ is the magnetic flux produced by a phase i flowing through a phase j winding; R_s is the inner stator radius; L_{axe} is the length of the ER-PMSM; K_w is the winding factor; $F_{distribution}$ is the distribution function of the machine; $\wp$ is air-gap permeance; F_w is the winding function; θ_s is the angular position in relation to the stator reference axis.

REFERENCES

[1] M. F. Tariq, A. Q. Khan, M. Abid, and G. Mustafa, "Data-Driven Robust Fault Detection and Isolation of Three-Phase Induction Motor," IEEE Trans. Ind. Electron., vol. 66, no. 6, pp. 4707–4715, Jun. 2019, doi: 10.1109/TIE.2018.2866104.

[2] H. Henao et al., "Trends in Fault Diagnosis for Electrical Machines: A Review of Diagnostic Techniques," IEEE Ind. Electron. Mag., vol. 8, no. 2, pp. 31–42, Jun. 2014, doi: 10.1109/MIE.2013.2287651.

[3] J. He, C. Somogyi, A. Strandt, and N. A. O. Demerdash, "Diagnosis of stator winding short-circuit faults in an interior permanent magnet synchronous machine," in 2014 IEEE Energy Conversion Congress and Exposition (ECCE), Sep. 2014, pp. 3125–3130. doi: 10.1109/ECCE.2014.6953825.

[4] A. Belkhadir, D. Belkhayat, Y. Zidani, R. Pusca, and R. Romary, "Torque Ripple Minimization Control of Permanent Magnet Synchronous Motor using Adaptive Ant Colony Optimization," in 2022 8th International Conference on Control, Decision and Information Technologies (CoDIT), May 2022, pp. 629–635. doi: 10.1109/CoDIT55151.2022.9804127.

[5] T. Orlowska-Kowalska et al., "Fault Diagnosis and Fault-Tolerant Control of PMSM Drives–State of the Art and Future Challenges," IEEE Access, vol. 10, pp. 59979–60024, 2022, doi: 10.1109/ACCESS.2022.3180153.

[6] D. Toumi, M. Boucherit, and M. Tadjine, "Observer-based fault diagnosis and field oriented fault tolerant control of induction motor with stator inter-turn fault," Arch. Electr. Eng., vol. 61, no. 2, pp. 165–188, Jun. 2012, doi: 10.2478/v10171-012-0015-1.

[7] F. L. T. Guefack, A. Kiselev, and A. Kuznietsov, "Improved Detection of Inter-turn Short Circuit Faults in PMSM Drives using Principal Component Analysis," in 2018 International Symposium on Power Electronics, Electrical Drives, Automation and Motion (SPEEDAM), Jun. 2018, pp. 154–159. doi: 10.1109/SPEEDAM.2018.8445403.

[8] A. Belkhadir, R. Pusca, D. Belkhayat, R. Romary, and Y. Zidani, "Analytical Modeling, Analysis and Diagnosis of External Rotor PMSM with Stator Winding Unbalance Fault," Energies, vol. 16, no. 7, p. 3198, Apr. 2023, doi: 10.3390/en16073198.

[9] B. Vaseghi, N. Takorabet, and F. Meibody-Tabar, "Fault Analysis and Parameter Identification of Permanent-Magnet Motors by the Finite-Element Method," IEEE Trans. Magn., vol. 45, no. 9, pp. 3290–3295, Sep. 2009, doi: 10.1109/TMAG.2009.2022156.

[10] B. Vaseghi, B. Nahid-mobarakh, N. Takorabet, and F. Meibody-Tabar, "Inductance Identification and Study of PM Motor With Winding Turn Short Circuit Fault," IEEE Trans. Magn., vol. 47, no. 5, pp. 978–981, May 2011, doi: 10.1109/TMAG.2010.2083639.

[11] L. Cava, C. Picardi, and F. Ranieri, "Application Of The Extended Kalman Filter To Parameter And State Estimation Of Induction Motors," Int. J. Model. Simul., vol. 9, no. 3, pp. 85–89, Jan. 1989, doi: 10.1080/02286203.1989.11760075.

[12] Y. Azzoug et al., "An Active Fault-Tolerant Control Strategy for Current Sensors Failure for Induction Motor Drives Using a Single Observer for Currents Estimation and Axes Transformation," Eur. J. Electr. Eng., vol. 23, no. 6, pp. 467–474, Dec. 2021, doi: 10.18280/ejee.230606.

AUTHORS' INFORMATION

Ahmed Belkhadir receveid the M.S. degree in electrical engineering and renewable energy in 2020 from Cadi Ayyad University, Marrakesh, Morocco. He is actually pursuing Ph.D. studies in the Laboratory of Electrical Systems and Environment (LSEE), Artois University, Béthune, France, and the Laboratory of Electrical Systems, Energy Efficiency and Telecommunications (LSEEET), Cadi Ayyad University, Marrakesh, Morocco. His research interest concerns the control and diagnosis of electrical machines.

Remus Pusca was born in Medias, Romania, in 1972. He received his Dipl. Ing. and M.S. degree in electrical engineering from the Technical University of Cluj-Napoca (UTCN), Cluj-Napoca, Romania, in 1995 and 1997, respectively. From 1997 to 1998, he was an Assistant Research Worker with the Department of Heat Treatment and Thermal Equipment, UTCN. From 1999 to 2003, he was a Research Worker with the Centre Recherche Electrotechnique Electronique Belfort. He obtained his Ph.D. degree in Electrical Engineering from the University of Franche-Comté, France in 2002. Since 2003, he is Assistant Professor at University of Artois, and a Member of the Team Research of the Laboratory of Electrical Systems and Environment (LSEE), Bethune, France. His knowledge in the field of diagnosis applied to electric machines were developed by working with the LSEE team specialized in this field. His current research interests include control of electrical systems and diagnosis of electrical machines.

Raphaël Romary (Member, IEEE) received the Ph.D. from Lille University, Lille, France, in 1995 and the D. SC degree from Artois University, Béthune, France, in 2007. He is currently a Full Professor in Artois University and a Researcher at the Laboratory of Electrical Systems and Environment (LSEE). His research interest concerns the analytical modeling of electrical machines with applications to noise and vibration, losses, electromagnetic emissions, diagnosis.

Driss Belkhayat was born in 1967 in Fez, Morocco. He did his graduate studies at Orsay University (PARIS XI) before continuing at the Ecole Normale Supérieure of Cachan in Paris. He received his PhD in 1993 from LILLE I University. In 2004, he received his State PhD in Electrical Engineering in his native country at Cadi Ayyad University (UCA) in Marrakesh. He is currently a Full Professor in Cadi Ayyad University, Researcher and Director of the Laboratory of Electrical Systems, Energy Efficiency and Telecommunications (LSEEET) of the Faculty of Sciences and Techniques of Marrakesh and Director of InnovTech doctoral center grouping 20 UCA research structures. His research field concerns electrical machines noise and vibrations reduction, numerical modeling and theoretical approaches by oriented control, the diagnosis and machine control methods.

Youssef Zidani was born in 1972, he received in 1994 his Diploma of Hight School Teachers degree in Electrical Engineering from ENSET (Rabat, Morocco). In 1997 and 2004 he received respectively the MSA and PhD degrees in Electrical Engineering and Power Electronics from Mohamed V University (Mohammadia School of Engineers, EMI, Rabat). In 2017, he received the Habilitation diploma from Cadi Ayad University. From 1994-2004, he was an Assistant Professor at Hight School of Technology (EST, Mohamed 1st University, Oujda). In 2004, he joined the Department of Applied Physics in the Faculty of Science and Technology (FST, Cadi Ayad University, Marrakesh) where he is actually a permanent Professor. His research interests are Electrical machines, Power electronics and Renewable energy.